©2025 Published in 11th International Symposium on Intelligent Technologies in Engineering and Science 16-18 May 2025 (ISITES2025 Diyarbakır - Turkey)

# PSO-Tuned Sliding Mode Control for Three-Phase Grid-Connected NPC Inverter

*[1]Muhammet Cengiz, [1]Tugrulhan Akgul, [1]Turgay Duman and [1]Ali Unluturk
[1]Department of Electrical and Electronics Engineering, Erzurum Technical University, 25100, Erzurum, Turkiye

## Abstract

This paper proposes a control strategy based on the integration of proportional resonance (PR) and sliding mode control (SMC) for a three-phase LCL-filtered grid-connected NPC inverter. The PR control generates the capacitor voltage reference thanks to its excellent AC signal tracking capability, while the SMC control regulates the grid current. The control parameters were determined by a metaheuristic algorithm called particle swarm optimization (PSO). In the applied SMC method, the sliding surface function of phase c is derived from phases a and b. In this way, the number of sensors is reduced by removing the necessity to measure the capacitor voltage for phase c. Moreover, the chattering is effectively reduced, and a constant switching frequency is ensured by the correction applied to the sliding surface function within a narrow boundary layer. Simulation results are presented to validate the high performance of the proposed method in both steady-state and dynamic conditions, as well as its robustness against disturbances.

**Key words:** Grid-connected inverter, three-phase NPC inverter, proportional resonance control, sliding mode control, particle swarm optimization

## 1. Introduction

The rapidly growing electricity demand, limited fossil fuel reserves, price fluctuations, and environmental concerns have significantly heightened interest in renewable energy sources. Accordingly, grid configuration to accommodate the rapidly growing integration of renewable energy sources is also gaining attention. Grid-connected inverters are essential components that play a crucial role in integrating DC power-generating renewable energy sources into the grid [1]. These inverters are generally classified into two-level and multi-level structures. Although conventional two-level inverters are cost-effective and have a simple structure, they have certain drawbacks, including the need for large output filters due to high total harmonic distortion (THD), significant voltage variation (*dv/dt*) on the switches, and a high switching frequency requirement [2]. In contrast, multilevel inverters outperform conventional inverters by offering advantages such as low THD at output voltages, lower *dv/dt* ratio, and low switching frequency.

Neutral point clamped (NPC) [3], flying capacitor (FC) [4], and cascaded H-Bridge (CHB) [5] multilevel inverter topologies are well-established and widely used configurations. These topologies have distinct advantages and disadvantages [6]. In the CHB inverter, an increased number of DC sources is required to increase the number of levels. Similarly, in the FC inverter, the number of capacitors rises with the increase in levels, making their voltage control more complex. NPC inverters can operate with a single DC source and can also achieve equivalent voltage levels using fewer components compared to FC inverters. Therefore, NPC inverters are widely accepted in grid-connected applications [7-9]. Another critical issue in grid-connected

*Corresponding author: Address: Department of Electrical and Electronic Engineering, Erzurum Technical University, 25100, Erzurum, Turkiye. E-mail address: muhammet.cengiz@erzurum.edu.tr

systems is the need for a well-designed current control method to be integrated into the inverter structure. The objectives of current control methods in grid-connected inverters can be summarized as follows: 1) to exhibit high steady-state performance, a fast dynamic response to sudden reference changes, and robustness against disturbances; 2) to inject a sinusoidal current with low THD into the grid; and 3) to maintain a constant switching frequency to minimize switching losses and facilitate the easy design of output filters [7, 10]. Various control methods have been proposed in the literature to achieve these objectives [11].

The SMC method stands out as an effective control strategy due to its fast dynamic response, high accuracy, robustness against disturbances, and simplicity [8-10]. Moreover, thanks to its switching logic, it can operate in natural harmony with power converters, which are variable structure systems. However, the main limitations to the implementation of SMC are as follows: 1) the chattering phenomenon caused by the discontinuity of the control structure, and 2) the variable switching frequency resulting from this phenomenon [9]. To reduce the effect of chattering to acceptable levels, various studies have been presented on hysteresis modulation-based (HM-SMC) [12,13] and pulse width modulation-based (PWM-SMC) [8-10] approaches. The HM-SMC approaches presented in [11, 12] can partially reduce the chattering effect and cannot eliminate the problem of variable switching frequency. In [8], the chattering effect is effectively reduced using an SMC approach integrated with the super-twisting algorithm (STA). However, the dependency of STA's control parameters on the derivative of the disturbance makes it quite challenging to determine the parameter bounds [14]. In [9, 10], the discontinuous control signal is made continuous within a boundary layer of thickness $\phi$ to reduce the chattering effect. While chattering is effectively reduced in the boundary layer method, the parameter $\phi$ must be carefully chosen to balance between chattering reduction and control performance.

In this study, an SMC strategy combined with the boundary layer method is presented for a three-phase grid-connected NPC inverter with an LCL filter. The particle swarm optimization (PSO) algorithm is used to determine the parameters of the SMC. This approach offers a more effective solution compared to traditional trial-and-error-based parameter determination methods.

## 2. Three-Phase Grid-Connected NPC Inverter Description

Fig. 1 shows a three-phase NPC inverter connected to the grid with an LCL filter. The LCL filter consists of the inverter-side inductor (L1), capacitor (C), and grid-side inductor (L2) and is connected between the inverter and the grid to improve the quality of the grid current. The three-phase NPC inverter consists of three phase legs, each containing four power switches and two clamping diodes. The clamping diodes are connected to the midpoint of the DC bus capacitors to create a zero voltage level, thereby reducing the voltage stress on the switches. The voltage levels corresponding to the switching states of the three-phase NPC inverter are shown in Table 1. In this configuration, $S_{1a}$–$S_{3a}$ and $S_{2a}$–$S_{4a}$ form complementary switch pairs, and the same rule applies to the phase legs of phases b and c.

The mathematical model of the system represented in Fig. 1 can be defined as the following equations:

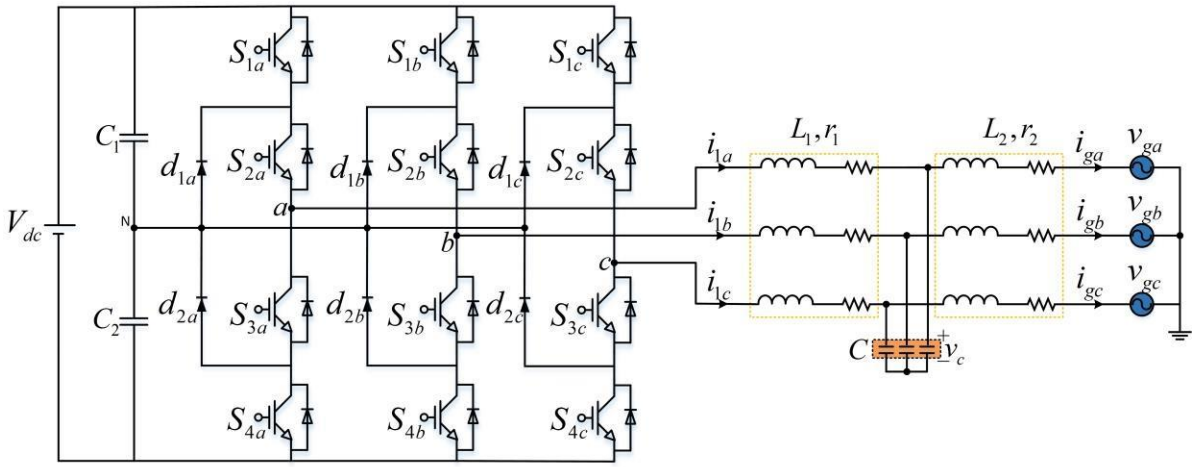


**Figure 1.** Three-phase grid-connected NPC inverter with LCL filter

$$L_1 \frac{di_{1m}}{dt} + r_1 i_{1m} = u_m V_{dc} - v_{cm} \tag{1}$$

$$L_2 \frac{di_{gm}}{dt} + r_2 i_{gm} = v_{cm} - v_{gm} \tag{2}$$

$$C \frac{dv_{cm}}{dt} = i_{1m} - i_{gm} \tag{3}$$

where $i_{1m} = [i_{1a}\ i_{1b}\ i_{1c}]^T$, $i_{gm} = [i_{ga}\ i_{gb}\ i_{gc}]^T$, $v_{cm} = [v_{ca}\ v_{cb}\ v_{cc}]^T$, and $v_{gm} = [v_{ga}\ v_{gb}\ v_{gc}]^T$, which represent inverter currents, grid currents, capacitor voltages, and grid voltages, respectively, while $u_m = [u_a\ u_b\ u_c]^T$ denotes the control inputs. The three-phase grid voltages are expressed as follows:

$$v_{ga} = V_g \sin(\omega t) \tag{4}$$

$$v_{gb} = V_g \sin(\omega t - 2\pi/3) \tag{5}$$

$$v_{gc} = V_g \sin(\omega t + 2\pi/3)\,. \tag{6}$$

It is generally expected that the grid current is in a sinusoidal form and is in phase with the grid voltage. Therefore, the grid current can be defined as follows, in accordance with the assumed grid voltages above.

$$i^*_{gm} = I_g \sin(\omega t + \theta) \tag{7}$$

where θ represents the phase shift, and for phases a, b, and c, it takes the values of 0, -2π/3, and 2π/3, respectively.

**Table 1.** Three-phase NPC inverter switching states

| State | $S_{1i}$ | $S_{2i}$ | $S_{3i}$ | $S_{4i}$ | Output voltage |
|---|---|---|---|---|---|
| 0 | 1 | 1 | 0 | 0 | $V_{dc}/2$ |
| 1 | 0 | 1 | 1 | 0 | 0 |
| 2 | 0 | 0 | 1 | 1 | $-V_{dc}/2$ |

## 3. PSO Tuned Sliding Mode Control Strategy

SMC operates based on a logic involving the reaching and sliding phases. Accordingly, its design comprises a sliding surface function and an appropriate control signal that drives the system states to reach and remain on the sliding surface. The sliding surface function can be defined as

$$S_m = \lambda x_1 + \dot{x}_1, \quad m = a,b,c \tag{8}$$

where $x_1$ denotes the state variable, $\dot{x}_1$ is its derivative, and $\lambda$ represents a positive sliding coefficient. The state variables can be expressed as [10]

$$x_{1a} = v_{ca} - v^*_{ca}, \quad x_{1a} = \frac{d}{dt}(v_{ca} - v^*_{ca}) \tag{9}$$

$$x_{1b} = v_{cb} - v^*_{cb}, \quad x_{1b} = \frac{d}{dt}(v_{cb} - v^*_{cb}) \tag{10}$$

where $v^*_{ca}$ and $v^*_{cb}$ denote the reference values of the capacitor voltage for phases a and b, respectively. $v^*_{ca}$ and $v^*_{cb}$ references are obtained using the PR control method, which ensures high-accuracy AC signal tracking. The transfer function of the PR control is defined as given in Eq. (11) [1]. As a result of the grid current errors applied to the input of the transfer function, the capacitor reference values are obtained at the output.

$$G_{PR}(s) = K_p + \frac{2K_r\omega_c s}{s^2 + 2\omega_c s + \omega^2} \tag{11}$$

where $K_p$ indicates the proportional gain, $K_r$ represents the resonance gain, and $\omega_c$ and $\omega$ correspond to the cutoff and resonance frequencies, respectively. In a three-phase system, since the voltage and currents are linearly related, the sliding surface function can be expressed as $S_a+S_b+S_c = 0$. Therefore, for the c-phase, the sliding surface function can be expressed as $S_c = -(S_a+S_b)$, utilizing the a and b phases. When the system is in the sliding phase, the sliding surface is mathematically defined by the equation $S = 0$. In this case, the solution of Eq. (8) is given as [9,10]

$$x_1(t) = x_1(0)e^{-\lambda t}. \tag{12}$$

As can be clearly observed from Eq. (12), for $\lambda > 0$, the state variable on the sliding surface converges to zero. Additionally, to ensure that the state variables continue to move along the sliding surface, the condition given in Eq. (13) must be satisfied.

$$S_m \dot{S}_m < 0 \tag{13}$$

where $\dot{S}$ represents the derivative of the sliding surface function. Now, the control input that satisfies the condition in Eq. (13) is defined as

$$u_m = -K sign(S_m), \quad m = a,b,c \tag{14}$$

where $K$ represents the control gain. As previously mentioned, the discontinuous nature of the *sign* function used in the control structure leads to chattering. To reduce the chattering amplitude, the value of $K$ can be chosen smaller; however, this approach compromises the robustness of the system against disturbances. Therefore, the sliding surface function is placed within a boundary layer of thickness $\phi$ instead of the *sign* function, and the control signal is obtained as shown in Eq. (15).

$$u_m = \frac{S_m}{\phi}, \quad m = a,b,c\,. \tag{15}$$

The control signal given in Eq. (15) is compared with triangular carriers to obtain the switching signals. To generate accurate switching signals, the slope of the carrier must be greater than the slope of the control signal. Based on this principle, the thickness of $\phi$ can be determined as follows. The details of this type of analysis can be found in [9].

$$\phi > \frac{V_{dc}}{8 L_1 C V_p f_{sw}} \tag{16}$$

where $V_p$ indicates the amplitude of the carrier signal, while $f_{sw}$ denotes its frequency. According to the above constraint, $\phi$ is adjusted using the PSO algorithm. The details of this algorithm are presented in the next section.

### *3.1.* Particle swarm optimization

PSO algorithm is a swarm intelligence-based optimization technique inspired by the social behavior of bird flocks or fish schools [15]. Based on multi-objective optimization [16] and binary optimization [17], the PSO algorithm is widely used in many different fields. In PSO, a swarm of particles moves in the search space to find the global best. Each particle has its own position and velocity, which are updated according to its individual best position and the global best position identified by the swarm, balancing exploration and exploitation to avoid premature convergence to local optima [18]. By adjusting their relative positions from one iteration to the next, a particle swarm enables the PSO algorithm to conduct the search process as intended. Each particle moves

towards its personal best position ($P^t_{best(i)}$) and the global best position in the swarm ($G^t_{best(i)}$) to obtain the best solution. The equations for ($G^t_{best(i)}$) and ($G^t_{best(i)}$) are given in Eq. (17) and (18).

$$p^t_{best(i)} = x^*_i \,\middle|\, f(x^*_i) = \min_{\substack{k=1,2,\ldots,t \\ i=1,2,\ldots,N}} \left( \left\{ f(x^k_i) \right\} \right) \tag{17}$$

$$g^t_{best(i)} = x^t_* \,\middle|\, f(x^t_*) = \min_{\substack{k=1,2,\ldots,t \\ i=1,2,\ldots,N}} \left( \left\{ f(x^k_i) \right\} \right) \tag{18}$$

Eq. (4) and (5) depict the index of particle *i*, the current iteration count *t*, the objective function *f* to be optimized (minimized), the position vector *x* (or a potential solution), and the total number of particles N in the swarm. The following equations update the velocity *v* and position *x* of each particle *i* in each *t+1* iteration.

$$v^{t+1}_i = w v^t_i + c_1 r_1 (p^t_{best(i)} - x^t_i) + c_2 r_2 (g^t_{best} - x^t_i) \tag{19}$$

$$x^{t+1}_i = x^t_i + v^{t+1}_i \tag{20}$$

where v represents the velocity vector, *x* is the inertia weight used to balance local exploitation and global exploration, $r_1$ and $r_2$ are uniformly distributed random vectors in the range [0, 1] (D denotes the dimensionality of the search space or the problem size), and $c_1$ and $c_2$ are positive constants referred to as acceleration coefficients. Eq. (19) can be interpreted as the initial part, referred to as the "inertial component," which represents the previous velocity that provides appropriate momentum for particles to explore the search space. Eq. (20) signifies the "cognitive component," reflecting the positivity for each particle, encouraging them to move towards their best positions discovered thus far in the subsequent iterations. The third part, known as the "social component," illustrates the collective influence of particles in achieving the global optimum solution.

PSO is a popular optimization technique that offers many advantages for designing controllers for various systems [19]. The most obvious advantages are fast convergence rate, easy implementation, stable convergence, and efficient computational efficiency [20]. In the proposed controller, the phase a grid current and phase b grid current errors average is defined as total error function (Eq. (21)).

$$e_1(t) = i^*_{ga} - i_{ga},\ e_2(t) = i^*_{gb} - i_{gb},\ e_T(t) = mean\left(e_1(t) + e_2(t)\right) \tag{21}$$

The objective function used in PSO, as given in Eq. (22), is selected Integral Time Absolute Error (ITAE), which is one of the error-based performance indices. ITAE has advantages such as less overshoot amount and settling time compared to its functions.

$$obj = \min\left( ITAE = \int_0^t t\,|e_T(t)| \right) \tag{22}$$

The upper and lower bounds of the search range for optimizing the control parameters are defined respectively as the limits of exploration in Eq. (23). The important parameters of the PSO algorithm used in the proposed controllers and the flowchart of the PSO algorithm are presented in Fig. 2. Fig. 3 shows the convergence curve of PSO finding the global optimum values of the objective function designed for the proposed controllers.

$$0.01 \le \lambda \le 20000, 125000 \le \phi \le 1250000, 0.1 \le K_p \le 50, 100 \le K_r \le 4500. \quad (23)$$

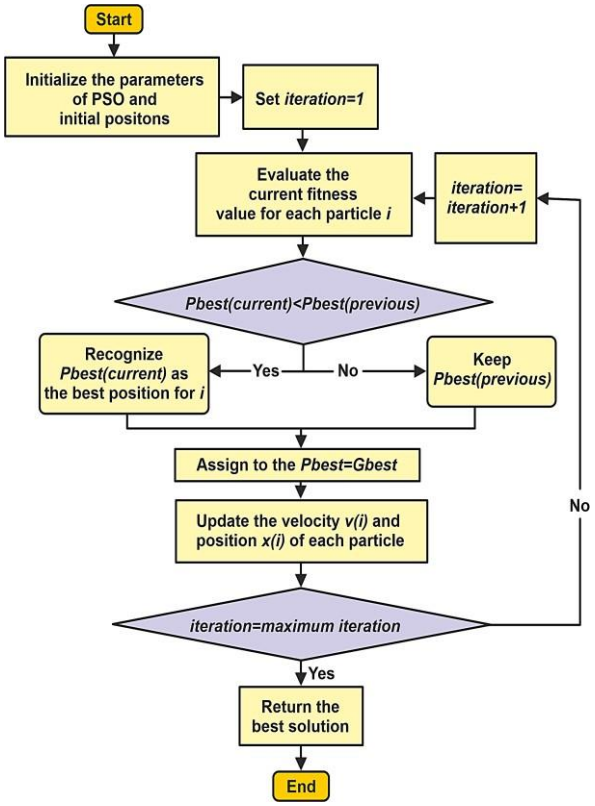


| Parameters | Proposed Controller |
|---|---|
| $c_1$ | 2 |
| $c_2$ | 2 |
| $w_{max}$ | 0.9 |
| $w_{min}$ | 0.2 |
| Population | 200 |
| Iteration | 5000 |
| Min ($g_{best}$) | 0.003087 |

**Figure 2.** Parameters and Flowchart of the PSO Algorithm [19].

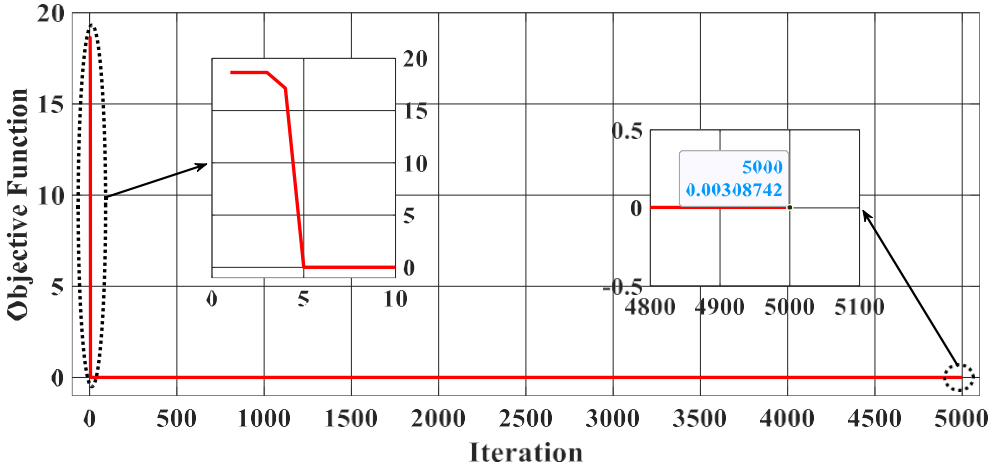


**Figure 3.** Convergence curve of objective function

## 4. Simulation Results

The proposed control method for the three-phase grid-connected NPC inverter has been tested using MATLAB/Simulink. The block diagram of the proposed control method is provided in Fig. 4. The control parameters are set as $\lambda = 5401.10$, $\phi = 177761.88$, $K_p = 9.91$, $K_r = 4377.15$, and $\omega_c = 1$ rad/s. The system parameters used in the simulation are listed in Table 2.

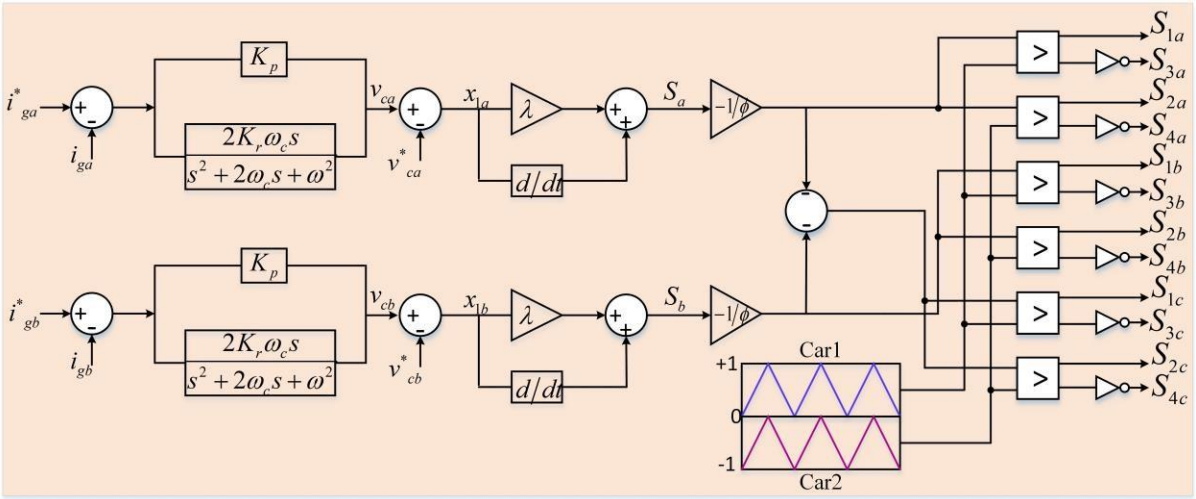


**Figure 4.** Block diagram of the proposed control method together with the PWM scheme

**Table 2.** System parameters.

| Parameter | Value |
|---|---|
| Grid voltage amplitude, $V_g$ | $230\sqrt{2}\ V$ |
| Inverter-side inductance, $L_1$ | *1.875 mH* |
| Grid-side inductance, $L_2$ | *0.61 mH* |
| Filter capacitance, $C$ | *20 μF* |
| DC bus voltage, $V_{dc}$ | *750 V* |
| Grid frequency, $f_g$ | *50 Hz* |
| Switching frequency, $f_{sw}$ | *20 kHz* |

Fig. 5 shows the waveforms of the grid voltages and currents under steady-state conditions. It is clearly observed that the grid currents are sinusoidal and balanced, and they are in phase with the grid voltages.

Fig. 6 illustrates the dynamic responses of the grid currents. As seen in the figures, the dynamic responses of the grid currents are fast under a sudden change in Ig. Additionally, the proposed control method is robust against disturbance effects. The phase-to-phase voltage of the inverter, as shown in Fig. 7, results in a five-level output.

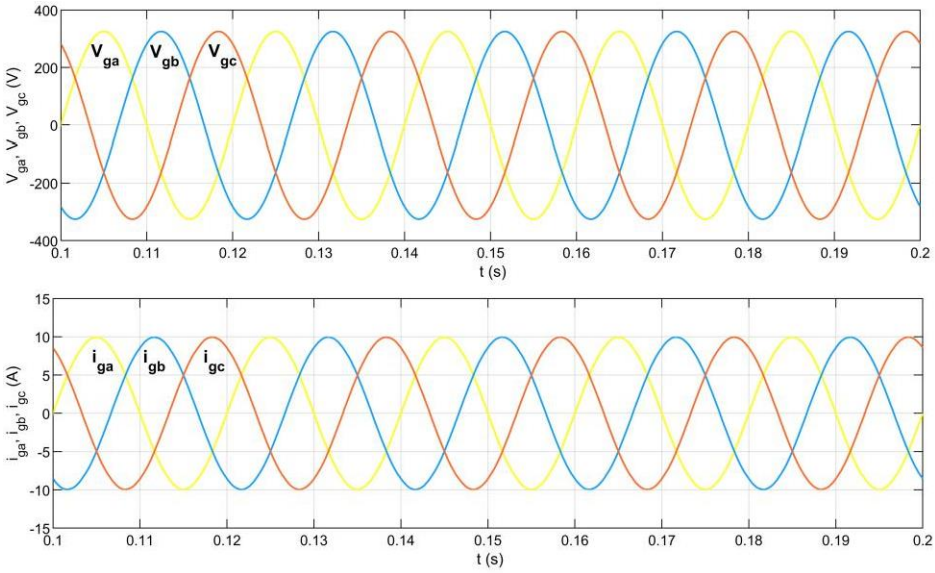


**Figure 5.** Three-phase grid voltages and currents in the steady state

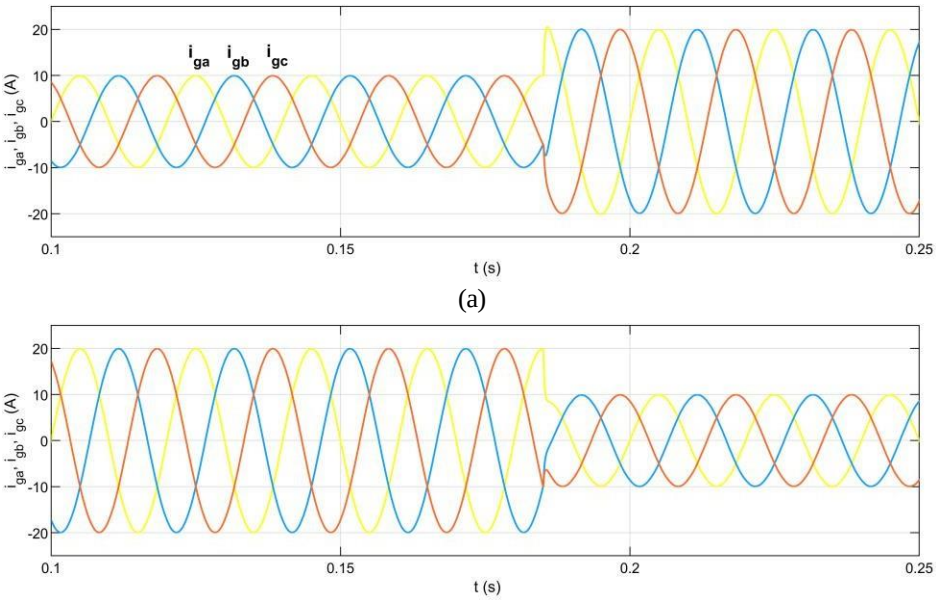


**Figure 6.** The dynamic responses of the grid currents: (a) a step change in $I_g$ from 10 to 20 A, (b) a step change in $I_g$ from 20 to 10 A

Fig. 8 shows the harmonic spectrum of the grid currents. The THDs of the grid currents are measured to be 0.34%, 0.34%, and 0.33%, respectively. This is evidence of the very low harmonic distortion in the grid currents.

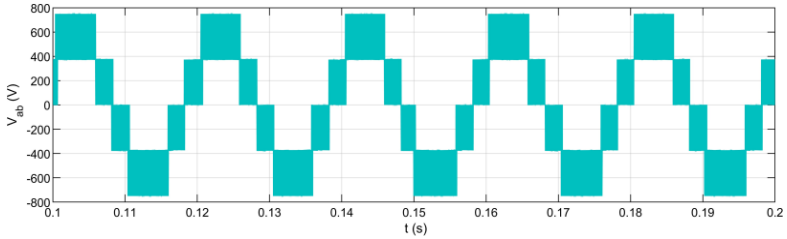


**Figure 7.** The inverter's phase-to-phase voltage

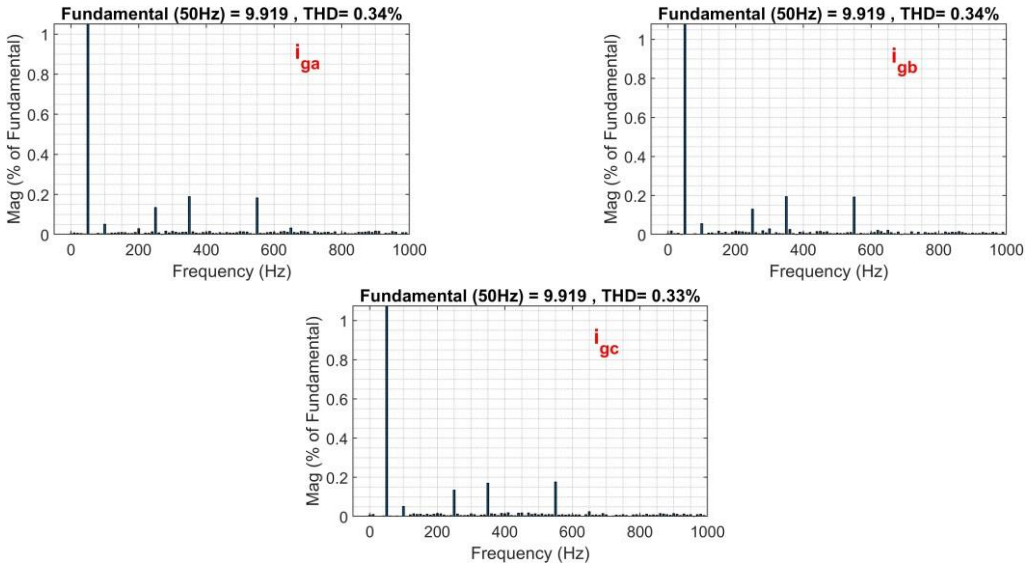


**Figure 8.** The harmonic spectrum of the grid currents

## Conclusions

In this study, an SMC method incorporating PR control is designed to control a three-phase grid-connected NPC inverter. The capacitor voltage reference was obtained using the PR control method, which reduces the steady-state error in the grid current. Accordingly, the sliding surface function was constructed based solely on the capacitor voltage error, with no additional grid current error incorporated into the sliding surface. Furthermore, the sliding surface function of phase c was derived from phases a and b, providing simplicity in the implementation. The simulation results show that all three-phase grid currents are balanced and exhibit very low total harmonic distortion. Additionally, it was validated that the proposed control method exhibits outstanding performance both under steady-state conditions and in the presence of disturbances.

## References

[1] Cengiz M, Duman T. Design and analysis of L and LCL filters for grid-connected HNPC inverters used in renewable energy systems. Balkan Journal of Electrical and Computer Engineering 2024;12(1):53-61.

[2] Kavya Santhoshi B, Mohana Sundaram K, Padmanaban S, Holm-Nielsen J B, KK P. Critical review of PV grid-tied inverters. Energies 2019;12(10):19-21.

[3] Nabae A, Takahashi I, Akagi H. A new neutral-point-clamped PWM inverter. IEEE Transactions on Industry Applications 1981;5:518-523.

[4] Meynard T A, Foch H. Multi-level conversion: high voltage choppers and voltage-source inverters. 23rd Annual IEEE Power Electronics Specialists Conference 1992;397-403.
[5] Peng F Z, Lai J S, McKeever J W, VanCoevering, J. A multilevel voltage-source inverter with separate DC sources for static var generation. IEEE Transactions on Industry Applications 1996;32(5):1130-1138.
[6] Vijeh M, Rezanejad M, Samadaei E, Bertilsson K. A general review of multilevel inverters based on main submodules: Structural point of view. IEEE Transactions on Power Electronics 2019;34(10):9479-9502.
[7] F. Sebaaly, H Vahedi, H Y Kanaan, N Moubayed, K Al-Haddad. Sliding Mode Fixed Frequency Current Controller Design for Grid-Connected NPC Inverter. IEEE Journal of Emerging and Selected Topics in Power Electronics 2019;4(4):1397-1405.
[8] N Altin, S Ozdemir, I Sefa, H Komurcugil. Second-Order Sliding Mode Control of Three-Phase Three-Level Grid-Connected Neutral Point Clamped Inverters. 13th International Conference on Electronics 2021;1-6.
[9] Cengiz M, Duman T. Sliding mode control for a single-phase grid-connected H-bridge NPC inverter with a symmetrical LCL filter. Computers and Electrical Engineering 2024;117:1092-98.
[10] H Komurcugil, S Bayhan. PI and Sliding Mode Based Control Strategy for Three-Phase Grid-Tied Three-Level T-Type qZSI. 45th Annual Conference of the IEEE Industrial Electronics Society 2019;5020-5025.
[11] M Ehab, C Townsend, H D Tafti, S Forouhari. A Review of Current Control Schemes in Grid Connected Inverters. 9th Southern Power Electronics Conference (SPEC) 2024;1-6.
[12] R Guzman, L G de Vicuña, M Castilla, J Miret, J de la Hoz. Variable structure control for three-phase LCL-filtered inverters using a reduced converter model. IEEE Trans. Ind. Electron 2018;65:5-15.
[13] O Kukrer, H Komurcugil, A Doganalp. A Three-Level Hysteresis Function Approach to the Sliding-Mode Control of Single-Phase UPS Inverters. IEEE Transactions on Industrial Electronics 2009;56(9):3477-3486.
[14] Utkin V, Poznya, A, Orlov Y, Polyakov A. Conventional and high order sliding mode control. Journal of the Franklin Institute 2020;357(15):10244-10261.
[15] M Clerc, J Kennedy. The particle swarm - explosion, stability, and convergence in a multidimensional complex space. IEEE Trans. Evol. Comput 2002;6(1):58-73.
[16] C A C Coello, G T Pulido, M.S Lechuga. Handling multiple objectives with particle swarm optimization. IEEE Trans. Evol. Comput. 2004;8:256-279.
[17] H N Pour, M R S S Babaki, M M Farsangi. Binary Particle Swarm Optimization: Challenges and New Solutions. The Journal of Computer Society of Iran (CSI) On Computer Science and Engineering (JCSE) 2008;6:21-32.
[18] A G Gad. Particle Swarm Optimization Algorithm and Its Applications: A Systematic Review. Arch. Comput. Methods Eng. 2022;29:2531–2561.
[19] T Akgul, A Unluturk. Comparison of PSO-LQR and PSO-PID Controller Performances on a Real Quarter Vehicle Suspension. 2023 Innovations in Intelligent Systems and Applications Conference (ASYU) 2023;1-6.
[20] X Sun, N Liu, R Shen, K Wang, Z Zhao, X Sheng. Nonlinear PID Controller Parameters Optimization Using Improved Particle Swarm Optimization Algorithm for the CNC System. Appl. Sci.;12(20):10269.